K.W. Li*, X.B. Wang, S.M. Li, W.X. Wang, S.P. Chen, D.Q. Gong and J.L. Cui

Halo Formation in Binary Fe-Nb Off-eutectic Alloys

Abstract: In the Fe-Fe_2Nb eutectic system, halo formations were observed at both the hypo- and hypereutectic compositions. This observation cannot be well explained by the existing halo theories based on competitive growth or competitive nucleating alone. In the present paper, a new explanation is proposed to describe the formation of halos in the binary Fe-Fe_2Nb off-eutectic alloys. By theoretical calculations, the α-Fe and Fe_2Nb are predicted to be the primary growing phase in the hypo- and hypereutectic compositions, respectively. Based on the experimental observations, the Fe_2Nb Laves phase was identified as a good nueleant for α-Fe phase, but not vice versa. By analysing of the competitive growth among the involved phases and the growth undercoolings of the two individual eutectic phases, the formation of halos in the Fe-Fe_2Nb alloys is explained successfully.

Keywords: halo, Laves phase, primary growing phase, competitive growth

PACS® (2010). 74.70.Ad, 81.30.Fb

DOI 10.1515/htmp-2014-0081
Received May 15, 2014; accepted August 10, 2014;
published online October 16, 2014

1 Introduction

Eutectic alloys formed by high melting point intermetallic phases are identified as potentially important materials to be utilized as structural materials due to their excellent mechanical properties and superior forming flexibility [1, 2]. Also, the eutectic alloys can be produced as in situ composites which are extensively used in practically industrial applications including casting, welding, soldering, etc. [3, 4].

In general, the microstructures of off-eutectic alloys comprise not only coupled eutectics, but also primary α or β dendrites under equilibrium solidification. However, the observation of a halo of one phase around a primary dendrite of another phase is a common occurrence during the solidification of off-eutectic alloys, which has been the subject of a considerable number of theoretical and experimental investigations [5–9]. By controlling the type and morphology of halo, the alloys with desired mechanical properties can be developed, similar to the deformation behavior of the ductile iron. However, the formation of halo in Laves phase alloys, which have been recognized as potential high-temperature structural materials, is still unknown and less understood. In this paper, the Fe_2Nb-based Laves phase alloys are chosen to study the halo formation, in which the occurrence of halo could be easily observed.

In the recent years, the Fe_2Nb Laves phase attracts increasing attention as the fine precipitates of Fe_2Nb Laves phase in steels can offer considerable strength and creep resistance at elevated temperatures [10–12]. Therefore, most of these investigations are focused on the effect of Fe_2Nb Laves phase on the mechanical properties of steels, due to its great potential for industrial applications. However, detailed experimental investigations on the solidification behavior of the Fe_2Nb C14 Laves phase and the formation mechanism of halo in the off-eutectic Fe-Nb alloys have not been reported previously.

This investigation is an attempt to understand the solidification behavior of the Fe_2Nb C14 Laves phase and the formation mechanism of halo in the off-eutectic Fe-Nb alloys. The microstructure evolution is discussed based on the competitive growth of involved phases at different solidification conditions.

2 Experimental

2.1 Alloy preparation

The alloys with nominal compositions of Fe-6%Nb and Fe-10%Nb were produced by arc melting with high purity

***Corresponding author: K.W. Li:** Key Laboratory of Interface Science and Engineering in Advanced Materials, Ministry of Education; College of Material Science and Engineering, Taiyuan University of Technology, Taiyuan 030024, China. E-mail: lkw917@126.com
X.B. Wang, W.X. Wang, S.P. Chen, D.Q. Gong: Key Laboratory of Interface Science and Engineering in Advanced Materials, Ministry of Education; College of Material Science and Engineering, Taiyuan University of Technology, Taiyuan 030024, China
S.M. Li: State Key Laboratory of Solidification Processing, Northwestern Polytechnical University, Xi'an 710072, China
J.L. Cui: Institute of Materials Engineering, Ningbo University of Technology, Ningbo 315016, China

metals (Nb: 99.99 wt.% and Fe: 99.5 wt.%, hereafter, all compositions in this paper are given in at.%.) under a titanium-gettered argon atmosphere. The samples were flipped and remelted five times to ensure chemical homogeneity. In the arc melting process, the melting current and time were kept in the ranges of 500 A and 60 s, respectively. Finally, several hemispherical ingots of about 90 g in weight and 35 mm in diameter were produced. The compositions of the as-cast ingots were analyzed by the inductively coupled plasma mass spectrometer (ICP-MS). The results indicated that the compositions in different position of the ingot were close to the nominal value for the element with the deviation less than 0.51 at.% for Fe, indicating negligible losses during processing.

2.2 Microstructure characterization

Three columnar samples of 5 mm in diameter were cut from the central region of different ingots by EDM. Then, these samples were cut longitudinally, ground, polished and etched for microstructure analyze. A scanning electron microscopy (SEM, JSM-6390A) equipped with an energy dispersive spectrometer were employed to identify the phases in the samples and characterize the microstructures.

3 Results and discussion

Fig. 1 shows the equilibrium phase diagram of the binary Fe-Nb system [13]. According to the phase diagram, the Fe-6%Nb and Fe-10%Nb alloys lie within the hypo- and hypereutectic areas, respectively. Thus, the sequence of phase formation in the Fe-6%Nb alloy is:

$$L_1 \rightarrow \delta\text{-Fe} + L_2$$
$$L_2 \rightarrow \delta\text{-Fe} + Fe_2Nb$$
$$\delta\text{-Fe} \rightarrow \gamma\text{-Fe} \rightarrow \alpha\text{-Fe}$$

while the sequence of phase formation in the Fe-10%Nb alloy is:

$$L_1 \rightarrow Fe_2Nb + L_2$$
$$L_2 \rightarrow \delta\text{-Fe} + Fe_2Nb$$
$$\delta\text{-Fe} \rightarrow \gamma\text{-Fe} \rightarrow \alpha\text{-Fe}$$

The primary solidified phase is δ-Fe or Fe_2Nb, and then the eutectic structure of δ-Fe + Fe_2Nb forms. At the end of solidification, the δ-Fe phase transforms into α-Fe through polytypic transformation. This information will help us understand the solidification of this binary system and the resultant microstructure, which governs their properties and ultimately their performance in service.

Fig. 2 illustrates the X-ray diffraction patterns of the samples taken from the as-cast Fe-6%Nb and Fe-10%Nb alloys. The indexation of different peaks in Fig. 2 confirms the presence of BCC ferrite and C14 Fe_2Nb, which agrees well with the prediction by the phase diagram showing in Fig. 1. Combined with the bulk composition measurements, it can conclude that there are no macrosegregation in the as-cast ingots.

Fig. 3 illustrates the typical SEM micrographs of the as-cast Fe-6%Nb and Fe-10%Nb alloys. Backscatter elec-

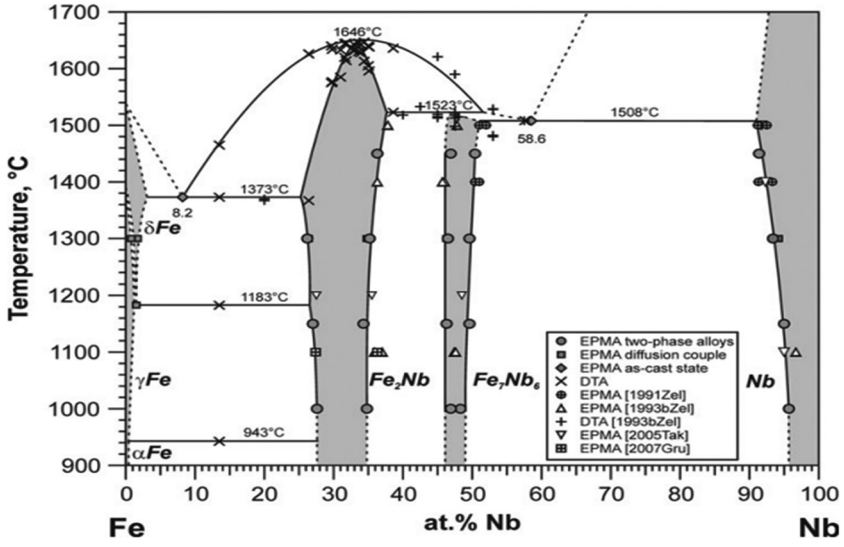

Fig. 1: Phase diagram of the binary Fe-Nb system [13]

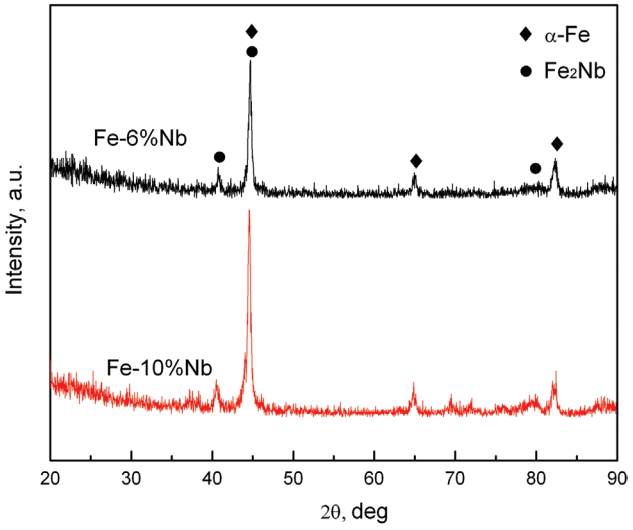

Fig. 2: X-ray diffraction patterns of (a) the as-cast Fe-6%Nb and (b) Fe-10%Nb

tron (BSE) imaging showed that the dark phase was the Fe phase and the light phase was the Fe_2Nb Laves phase, which was confirmed by the following composition analysis using energy dispersive X-ray spectrometry (EDS). Note that the primary Fe phase exhibits typically dendritic morphology and were surrounded by Fe_2Nb halos, and then the eutectic structure grew over it (Fig. 3b). Similarity, a halo of Fe surrounded the Fe_2Nb primary phase and generally separated it from the coupled eutectic (Fig. 3d). However, the primary Fe_2Nb Laves phase shows neither typically faceted nor completely dendritic morphology.

Table 1: The experimentally measured lamellar spacing in the Fe-Nb alloys

	Minimum λ_{min}	Maximum λ_{min}	Average λ_{ave}
Fe-6%Nb	0.31	0.83	0.56
Fe-10%Nb	0.95	2.22	1.95

Furthermore, the width of Fe halo is much larger than that of the Fe_2Nb halo. However, the lamellar spacing of eutectic in the Fe-6%Nb hypoeutectic alloy is far smaller than that of the Fe-10%Nb hypereutectic alloy as shown in Table 1.

The formation of halos in off-eutectic systems has been examined by many researchers [5, 8, 9, 14], and halo formation in equiaxed solidification were found to be related with the undercoolings required for the nucleation of primary phase and eutectic, and the growth velocities of the involved phases [15, 16].

As for the nucleating model, in the alloy with the composition of C_1, the primary β phase will precipitate from the liquid at some temperature below the liquidus, T_1, as shown in Fig. 4a. The liquid composition will follow the extension of the liquidus line to a temperature T_2 and composition C_2. If β phase is a poor nucleant of α, the temperature T_2 and composition C_2 can be significantly below the

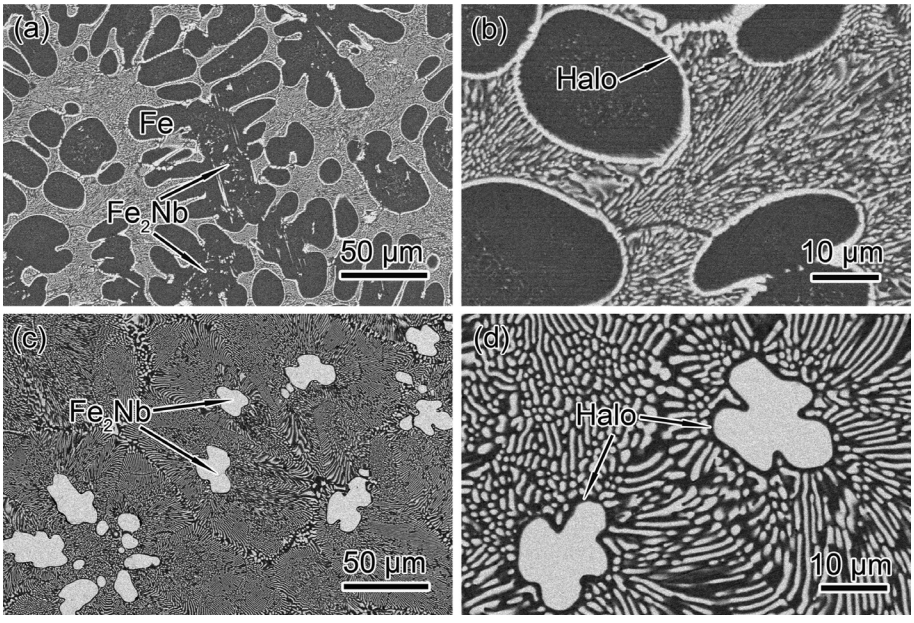

Fig. 3: Typical scanning electron micrographs of (a) the Fe-6%Nb and (c) the Fe-10%Nb. (b) and (d) are the enlarged figures of (a) and (c), respectively.

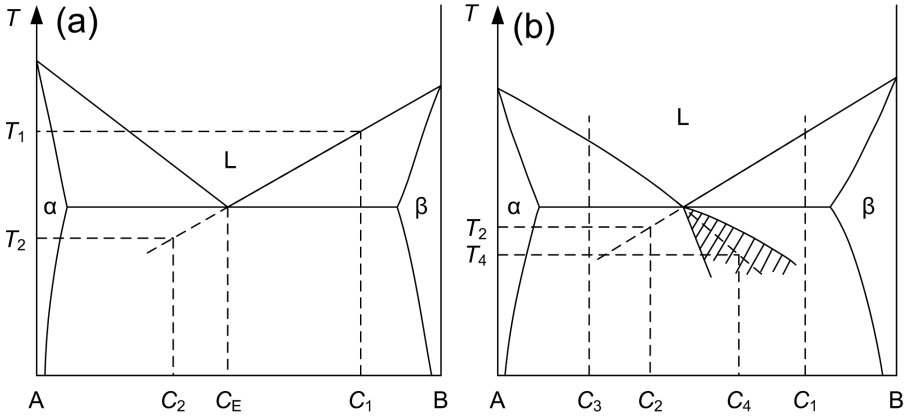

Fig. 4: Hypothetical phase diagram showing (a) the nucleating model and (b) the growth model [17]

eutectic temperature T_E and the eutectic composition C_E. In this condition, a halo of α phase will form about the primary β phase as the remaining liquid is supersaturated in element A. With the growth of α halo and release of latent heat by α halo, the liquid composition and temperature shift back to C_E and T_E, respectively, where the coupled eutectic growth begins.

According to the nucleating model, halos should exist only when the primary phase is not a good nucleant of the second phase. For the faceted-nonfaceted eutectic systems, the nucleating abilities of the two phases are sharply different. In general, the faceted phase is a good nucleant while the nonfaceted phase is a poor nucleant [17, 19]. Thus, halos can be formed only in the Fe-6%Nb hypoeutectic alloy rather than the Fe-10%Nb hypereutectic alloy. However, this conclusion is inconsistent with the experiment results of this study, in which halos form in both the hypo- and hypereutectic regions.

As for the growth model, the formation of halos was explained in terms of the coupled eutectic zone rather than undercooling considerations. As shown in Fig. 4b, for the alloy with composition of C_1, a halo of α phase will develop since the temperature T_2 and composition C_2 lie without the coupled eutectic zone. Conversely, for an alloy of composition C_3, a halo of β phase cannot develop around primary α phase since the extension of the liquidus line lies within the coupled zone, where the coupled eutectic growth can begin immediately.

In such case, the emphasis is focused on the distribution of the coupled eutectic zone of the Fe-Fe_2Nb alloy system, which can be plotted by comparing the interface growth temperatures of primary phase and coupled eutectic. In this paper, the TMK [17] and BCT models [18], which have been proved to be the most successful models for describing the eutectic and the dendrite growth, are employed to calculate the interface growth temperatures of coupled eutectic and primary phase.

For the TMK eutectic growth model, it presents the ΔT-V-λ interrelationship by the following two equations:

$$\lambda^2 V = \alpha^L / Q^L \tag{1}$$

$$\lambda \Delta T = m\alpha^L \left[1 + \frac{P}{P + \lambda\left(\partial P / \partial \lambda\right)} \right] \tag{2}$$

where λ is the lamellar spacing, ΔT is the non-equilibrium undercooling, and the definitions of the other terms are as follows:

$$\alpha^L = 2\left[\frac{\alpha_\alpha^L}{f m_\alpha} + \frac{\alpha_\beta^L}{(1-f) m_\beta} \right] \tag{3}$$

$$Q^L = \frac{1-k}{f(1-f) D_L} \left[P + \lambda(\partial P / \partial \lambda) \right] \tag{4}$$

$$P(f,p) = \sum_{n=1}^{\infty} \frac{1}{(n\pi)^3} \left[\sin(n\pi f) \right]^2 \cdot \frac{p_n}{1 + \sqrt{1 + p_n^2}} \quad (n = 1,2,3\ldots) \tag{5}$$

$$P + \lambda\left(\partial P / \partial \lambda\right) = \sum_{n=1}^{\infty} \left(\frac{1}{n\pi} \right)^3 \left[\sin(n\pi f) \right]^2 \times \left[\frac{p_n}{1 + \sqrt{1 + p_n^2}} \right]^2 \cdot \frac{p_n}{\sqrt{1 + p_n^2}} \quad (n = 1,2,3\ldots) \tag{6}$$

where $p_n = 2n\pi / Pe$, $Pe = V\lambda / 2D_L$, f is the volume fraction of the α-Fe in the α-Fe+Fe_2Nb eutectic, α_α^L and α_β^L are the capillarity constants of Fe and Fe_2Nb, P_e is the solutal Peclet number, D_L is the liquid diffusion coefficient, m is the liquidus slope, k is the solute distribution coefficient.

Also, the relationship between dendrite growth velocity V and undercooling ΔT in the BCT dendritic growth model is determined by the following two coupled equations:

$$\Delta T = \Delta T_t + \Delta T_C + \Delta T_r + \Delta T_K \tag{7}$$

where ΔT represents the total undercooling, ΔT_t the thermal undercooling, ΔT_C the solute undercooling, ΔT_r the curvature undercooling, and ΔT_K the kinetic undercooling. The terms of Eq. (7) have the following meanings:

(i) The thermal undercooling

$$\Delta T_t = \frac{\Delta H}{C_P} \cdot Iv\left(P_T\right) \tag{8}$$

where $Iv(P) = P\exp(P)E_1(P)$ is the Ivantsov function, in which $E_1(P)$ is the exponential integral function, ΔH is the heat of fusion, C_P the specific heat of the liquid phase.

(ii) The solute undercooling

$$\Delta T_C = m_L C_0 \left[1 - \frac{m'/m_L}{1-\left(1-k\right)Iv\left(P_C\right)}\right] \tag{9}$$

in which the parameter m' and k can be expressed as follows:

$$m' = m_L\left[1 + \frac{k_0 - k\left(1-\ln\left(k/k_0\right)\right)}{1-k_0}\right] \tag{10}$$

$$k = \frac{k_0 + \left(a_0/D_L\right)V}{1+\left(a_0/D_L\right)V} \tag{11}$$

where m_L' is the actual liquidus slope under non-equilibrium conditions, k the actual solute partition coefficient, m_L the slope of α-Cr liquidus, a_0.

(iii) The curvature undercooling

$$\Delta T_r = \frac{2\Gamma}{R} \tag{12}$$

$$R = \frac{\sigma/\left(\Delta S \cdot \sigma^\star\right)}{\frac{P_t \Delta H}{C_P}\xi_t + \frac{2m'P_C C_0\left(k-1\right)}{1-\left(1-k\right)Iv\left(P_C\right)}\xi_C} \tag{13}$$

in which the solute stability function ξ_t and the thermal stability function ξ_C were expressed as follows:

$$\xi_t = 1 - \frac{1}{\sqrt{1+\frac{1}{\sigma^\star \cdot P_t^2}}} \tag{14}$$

$$\xi_C = 1 + \frac{2k}{1-2k-\sqrt{1+\frac{1}{\sigma^\star \cdot P_C^2}}} \tag{15}$$

where Γ is the Gibbs-Thomson coefficient, $\sigma^\star$ the stability constant, P_t the thermal Peclet number, P_c the solute Peclet number.

(iv) The kinetic undercooling

$$\Delta T_K = \frac{V}{\mu} \tag{16}$$

in which the kinetic factor $\mu = \frac{\Delta H V_0}{R T_L^2}$, T_L is the liquidus temperature, R the gas constant, V_0 Sound velocity.

Using the physical parameters of Table 2 and solving the interface growth temperatures of primary phase and coupled eutectic, the coupled eutectic zone of the Fe-Fe_2Nb alloy system is given in Fig. 5. It can be seen that the coupled eutectic zone leans to the Fe_2Nb Laves phase side and the liquidus extension of α-Fe phase falls within this region. Thus, according to the halo growth model as described in Fig. 4b, α-Fe halos can be formed in the Fe-10%Nb hypereutectic alloy while Fe_2Nb halos cannot be formed in the Fe-6%Nb hypoeutectic alloy, which is inconsistent with the our experiment results.

Table 2: Physical parameters used for calculations in Fe-Nb alloys [13]

Physical parameter	Symbol (Unit)	Value
Eutectic growth		
Eutectic composition, Nb	C_E (at.%)	8.2
Eutectic temperature	T_E (K)	1646
Volume fraction of Fe phase	f_α	0.773
Equilibrium liquidus slope of α-Fe phase	m_α (K/at.%)	−15.116
Equilibrium liquidus slope of β-Fe_2Nb phase	m_β (K/at.%)	4.133
Capillarity constant of α-Fe phase	Γ_α (mK)	1.8×10^{-7}
Capillarity constant of β-Fe_2Nb phase	Γ_β (mK)	2.2×10^{-7}
Dendritic growth of β-Fe_2Nb phase		
Liquidus temperature	T_β (K)	1919
Diffusion coefficient	D_L (m^2/s)	3.5×10^{-9}
Heat of fusion	ΔH (J/mol)	79000
Sound velocity	V_0 (m/s)	5000
Specific heat of liquid	C_P (J/mol·K)	56.76

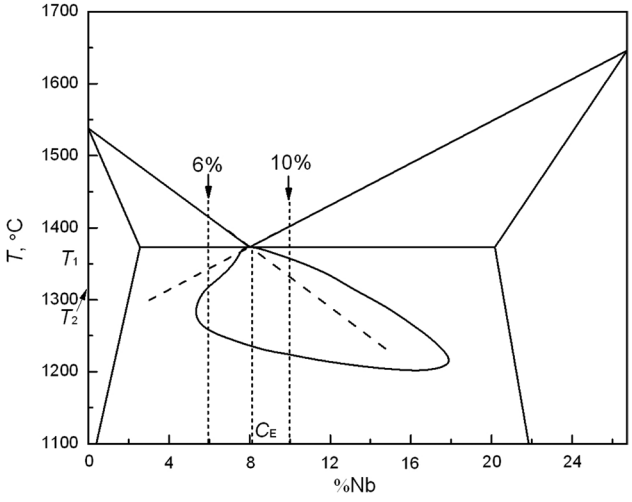

Fig. 5: The calculated coupled growth zone of the Fe-Fe_2Nb alloy system

Note that the previously proposed models of halo formation ignored the growth undercoolings of the two individual eutectic phases and assumed that eutectic reaction taken place immediately once the liquid composition entered the coupled growth zone. Actually, the two individual phases in the eutectic do not precipitate simultaneously and their growth undercoolings should be also taken into account. Combined with the experimental observations and the theoretical calculations, it is proposed that both the competitive growth among the involved phases and the growth undercoolings of the two individual eutectic phases control the halo formation in these experiments.

By employing the BCT model, the growth rates of α-Fe and Fe_2Nb phases in Fe-6%Nb hypoeutectic and Fe-10%Nb hypereutectic alloys are given in Fig. 6a and 6b. The α-Fe phase is indicated to be the primary growing phase in the Fe-6%Nb hypoeutectic alloy, while the Fe_2Nb Laves phase is primary growing phase in the Fe-10%Nb hypereutectic alloy.

For the Fe-6%Nb hypoeutectic alloy, the liquid composition can be significantly deviates the eutectic composition C_E as the Fe phase is a poor nucleant of Fe_2Nb phase. In this case, the liquid composition will fall within the coupled growth zone, which is convenient for the eutectic reaction. However, the eutectic growth cannot begin since considerable kinetic undercooling and growth undercooling are required for the precipitations of Fe_2Nb faceted phase and Fe nonfaceted phase, respectively. Thus, the Fe primary dendrites will grow rapidly in the undercooled melt. With the precipitation of Fe primary dendrites, the solute enrichment ahead the solid/liquid interface will be further enhanced and the liquid composition would move away from the coupled zone, which leads to the eutectic spacing in the Fe-6%Nb is far smaller than that of the Fe-10%Nb. Moreover, such a composition shift implies significant undercooling of Fe_2Nb without Fe_2Nb growth, an unstable situation. In this condition, the Fe_2Nb Laves phase grows as a halo to driven the liquid composition and temperature to C_E and T_E, where coupled growth can occur.

In the case of Fe-10%Nb hypereutectic alloy, the liquid composition decreases to C_1, which is slightly smaller than the eutectic composition, C_E, due to the rapid precipitation of primary Fe_2Nb phase [19]. As the eutectic growth cannot begin in this condition, the solute ahead the solid/liquid interface will be further enriched. Meanwhile, considering that the Fe_2Nb Laves phase is a good nucleant of Fe phase, the Fe phase will nucleate around the primary Fe_2Nb phase. Furthermore, the Fe phase would grow rapidly forming the Fe halos since the liquid composition

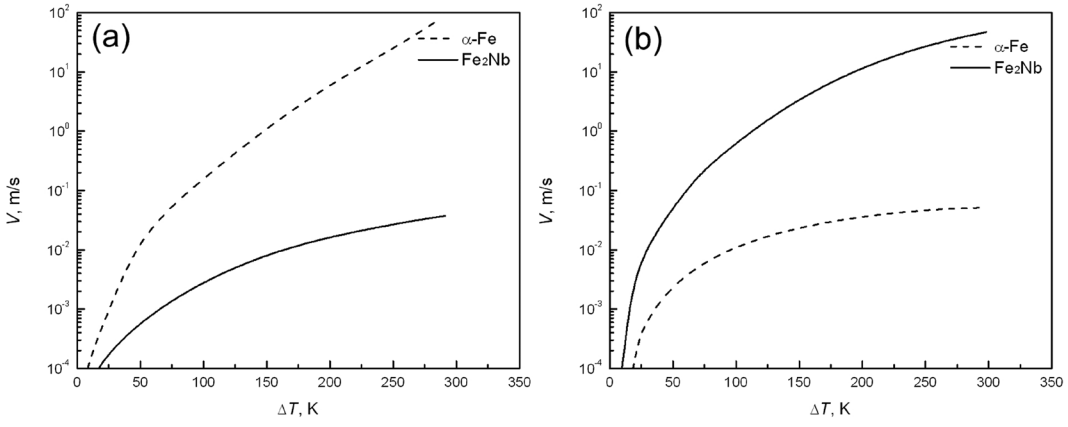

Fig. 6: The calculated relationships of ΔT-V in (a) the Fe-6%Nb and (b) Fe-10%Nb

and temperature lie without the coupled growth zone. With the formation of Fe halos, the liquid composition is driven to C_E, and then the coupled eutectic growth begins. Noting that the liquid composition C_1 is close to C_E, so the width of the Fe halo will be limited, which is in good agreement with the experimental results.

4 Conclusion

1. In the Fe-Fe_2Nb eutectic system, halos of Fe_2Nb Laves phase around the primary Fe dendrites were observed in the Fe-6%Nb hypoeutectic alloy, and Fe halos around the primary Fe_2Nb dendrites were also observed in the Fe-10%Nb hypereutectic alloy.
2. The α-Fe and Fe_2Nb Laves phase phases are predicted to be the primary growing phase in the Fe-6%Nb and Fe-10%Nb alloys, respectively. The Fe_2Nb Laves phase was identified as a good nueleant for α-Fe phase, but not vice versa.
3. The formation of halos in the Fe-Nb alloys is result in the competitive growth among the involved phases and the growth undercoolings of the two individual eutectic phases.

Funding: This research is financially supported by the National Science Fund for Young Scholars (No. 51101111) and the research project supported by Shanxi Scholarship Council of China (No. 2012-031), and the Qualified Personnel Foundation of Taiyuan University of Technology (tyut-rc201421a, tyut-rc201397a).

References

[1] J.E. Spinelli, B.L. Silva and A. Garcia, Mater Design, 58 (2014) 482–490.
[2] S. Balam and A. Paul, Metall. Mater. Trans. A, 41 (2010) 2175–2179.
[3] Z.R. Li, C.L. Ma, S.G. Tian, L.Q. Chen and X.H. Liu, High Temp. Mat. Pr., 33 (2013) 131–136.
[4] S. Çelik and I. Ersozlu, High Temp. Mat. Pr., 33 (2013) 161–170.
[5] M.D. Nave, A.K. Dahle and D.H. St. John, Acta Mater., 50 (2002) 2837–2849.
[6] K.W. Li, S.M. Li, Y.L. Xue and H.Z. Fu, J. Cryst. Growth, 357 (2012) 30–34.
[7] S.M. Li, B.L. Jiang, B.L. Ma and H.Z. Fu, J. Cryst. Growth, 299 (2007) 178–183.
[8] M.X. Gigliotti, G. Colligan and G.F. Powell, Metall. Trans., 1 (1970) 891–897.
[9] M.-J. Suk and K. Leonartz, J. Cryst. Growth, 213 (2000) 141–149.
[10] A.V. Kazantzis, M. Aindow, I.P. Jones, G.K. Triantafyllidis and J.Th.M. De Hosson, Acta Mater., 55 (2007) 1873–1884.
[11] T. Takasugi, M. Yoshida and S. Hanada, Acta Mater., 44 (1996) 669–674.
[12] K.S. Kumar and D.B. Miracle, Intermetallics, 2 (1994) 257–274.
[13] S. Voß, M. Palm, F. Stein and D. Raabe, J. Phase Equilib. Diff., 32 (2011) 97–104.
[14] S.M. Li, B.L. Jiang, B.L. Ma and H.Z. Fu, J. Cryst. Growth, 299 (2007) 178–183.
[15] S.T. Bluni, M.R. Notis and A.R. Marder, Acta Metall. Mater., 43 (1995) 1775–1782.
[16] B.E. Sundquist, R. Bruscato and L.F. Mondolfo, J. Aust. Inst. Met., 91 (1963) 204–206.
[17] R. Trivedi, P. Magnin and W. Kurz, Acta Metall., 35 (1987) 971–980.
[18] W.J. Boettinger, S.R. Coriell and R. Trivedi, In: R. Mehrabian (ed.), Proc. 4th Conf. on Rapid Solidification Processing, Principles and Technologies. Baton Rouge, LA: Claitors; 1987, p. 13.
[19] W. Kurz and D.J. Fisher, Fundamentals of Solidification, 4th edition, Trans Tech Publications Ltd, Switzerland, 2005.